The Cryosphere Discuss., doi:10.5194/tc-2015-225, 2016
Manuscript under review for journal The Cryosphere
Published: 19 January 2016

The Cryosphere Discussions
Open Access
EGU

MABEL photon-counting laser altimetry data in Alaska for ICESat-2 simulations and development

K. M. Brunt[1,2], T. A. Neumann[2], J. M. Amundson[3], J. L. Kavanaugh[4], M. S. Moussavi[5,6], K. M. Walsh[2,7], W. B. Cook[2], and T. Markus[2]

[1] {Earth System Science Interdisciplinary Center, University of Maryland, College Park, Maryland}

[2] {NASA Goddard Space Flight Center, Greenbelt, Maryland}

[3] {University of Alaska Southeast, Juneau, Alaska}

[4] {University of Alberta, Edmonton, Alberta, Canada}

[5] {Cooperative Institute for Research in Environmental Sciences (CIRES), University of Colorado, Boulder, Colorado}

[6] {National Snow and Ice Data Center (NSIDC), CIRES, University of Colorado, Boulder, Colorado}

[7] {Stinger Ghaffarian Technologies, Inc., Greenbelt, Maryland}

Correspondence to: K.M. Brunt (kelly.m.brunt@nasa.gov)

Abstract

Ice, Cloud, and land Elevation Satellite-2 (ICESat-2) is scheduled to launch in 2017 and will carry the Advanced Topographic Laser Altimeter System (ATLAS), which is a photon-counting laser altimeter and represents a new approach to satellite determination of surface elevation. Given the new technology of ATLAS, an airborne instrument, the Multiple Altimeter Beam Experimental Lidar (MABEL), was deployed in July 2014 to Alaska to provide data needed for satellite-algorithm development, simulating key elements of the photon-counting sampling strategy, and assessing elements of the resulting data that may vary seasonally. Here, we compare MABEL lidar data to *in situ* observations in Southeast Alaska to assess instrument performance in summer conditions

The Cryosphere Discuss., doi:10.5194/tc-2015-225, 2016
Manuscript under review for journal The Cryosphere
Published: 19 January 2016

and in the presence of glacier surface melt ponds and a wet snowpack. Results indicate that: 1) the ATLAS 90 m beam-spacing strategy will provide a robust assessment of across-track slope that is consistent with shallow slopes (<1°) of an ice-sheet interior over 50 to 150 m length scales; 2) the dense along-track sampling strategy of photon counting systems provides crevasse detail; and 3) MABEL 532 nm wavelength light may be sampling the surface and subsurface of shallow (approximately 2 m deep) supraglacial melt ponds.

1 Introduction

Ice, Cloud, and land Elevation Satellite-2 (ICESat-2) is a NASA mission scheduled to launch in 2017. ICESat-2 is a follow-on mission to ICESat (2003-2009) and will extend the time series of elevation-change measurements aimed at estimating the contribution of polar ice sheets to eustatic sea level rise. ICESat-2 will carry the Advanced Topographic Laser Altimeter System (ATLAS), which uses a different surface detection strategy than the instrument onboard ICESat. Specifically, ATLAS will be a 6-beam, photon-counting laser altimeter. In a photon-counting system, single-photon sensitive detectors are used, and the arrival time of any detected photon is recorded. ATLAS will use short (< 2 ns) 532 nm wavelength pulses, with a 10 kHz repetition rate, a ~14 m diameter footprint, and a ~70 cm along-track sampling interval (Abdalati et al., 2010). An accurate assessment of ice-sheet surface-elevation change based on altimetry is dependent upon knowledge of local slope (Zwally et al., 2011). Therefore, the six ATLAS beams are arranged into three sets of pairs. Spacing between the three pair sets is ~3 km to increase sampling density, while spacing between each beam within a given pair will be ~90 m to make the critical determination of local slope on each pass. Therefore, elevation change can be determined from only two passes of a given area (Abdalati et al., 2010; Brunt et al., 2014).

Given this new approach to satellite surface elevation measurement, an airborne instrument, the Multiple Altimeter Beam Experimental Lidar (MABEL), was developed to: 1) enable the development of ICESat-2 geophysical algorithms prior to launch; 2) enable ICESat-2 error analysis; and 3) provide ATLAS model validation. MABEL (discussed in detail in McGill et al., 2013) is a multibeam, photon-counting lidar,

The Cryosphere Discuss., doi:10.5194/tc-2015-225, 2016
Manuscript under review for journal The Cryosphere
Published: 19 January 2016

sampling at both 532 and 1064 nm wavelengths using short (~1.5 ns) laser pulses. MABEL beams are arranged approximately linearly, perpendicular to the direction of flight, with 1064 beams leading 523 beams by ~60 m. The system allows for beam-geometry changes between flights with a maximum beam spread of ±1 km from the 20 km nominal altitude of the NASA ER-2 aircraft. The laser pulse repetition rate is variable (5 to 25 kHz) and was 5 kHz for the data presented here. At this nominal altitude and repetition rate, and at an aircraft speed of ~200 m s^{-1}, MABEL samples a ~2 m footprint every ~4 cm along-track.

Following engineering test flights in 2010 and 2011, MABEL was deployed to Greenland (April 2012) and Alaska (July 2014) to collect data that included glacier targets. The Greenland 2012 campaign was intended to sample winter-like conditions while the Alaska 2014 campaign was timed to collect data during the summer melt season.

MABEL beam geometry, specifically the spacing between the individual beams, is adjustable but has generally been configured to allow simulation of the planned beam geometry of ATLAS. Previous results from the MABEL 2012 Greenland campaign suggest that the ATLAS beam geometry is appropriate for the determination of slope on ~90 m across-track length scales, a measurement that will be fundamental to deconvolving the effects of local surface slope from the ice-sheet surface-elevation change derived from ATLAS (Brunt et al., 2014).

Here, we compare *in situ* measurements with MABEL airborne lidar data on the Bagley (16 July 2014; 60.5° N, 141.7° W) and Juneau (31 July 2014; 58.6° N, 134.2° W) icefields in Southeast Alaska (Fig. 1). These comparisons are made with consideration for the ATLAS planned beam geometry to investigate instrument performance in summer conditions and in the presence of surface crevasses and melt ponds.

2 Data and methods

2.1 MABEL data

MABEL data (release 9) for the Alaska 2014 campaign (Fig. 1) are available from the NASA ICESat-2 website (http://icesat.gsfc.nasa.gov/icesat2/data/mabel/mabel_docs).

The Cryosphere Discuss., doi:10.5194/tc-2015-225, 2016
Manuscript under review for journal The Cryosphere
Published: 19 January 2016

Each data file contains 1 minute of data for every available beam (approximately two beams per deployment were compromised due to instrumentation issues). The data files contain photon arrival times resulting from reflected laser light (*i.e.*, signal photons), solar background and backscatter in the atmosphere (*i.e.*, background photons) and, to a lesser degree, detector noise (*i.e.*, noise photons). A histogram-based surface-finding algorithm developed at NASA Goddard Space Flight Center was used to discriminate signal photons from background and noise photons. Details of this surface-finding algorithm are described in Brunt et al. (2014). The derived surface elevations are reported relative to the WGS84 ellipsoid.

MABEL beams have non-uniform transmit energy. This is because all beams originate from a single laser source, but once the source is split into the individual beams, each beam follows a unique optical path through the instrument. The laser source is of 1064 nm wavelength; part of this source beam is divided into a series of 1064 nm beams while the rest of the source beam is frequency-doubled and then divided into a series of 532 nm beams (McGill et al., 2013). Owing to the frequency-doubling process and the non-uniform optical paths through the instrument, the 1064 nm and 523 nm transmit-pulse shapes are generally not the same. Although MABEL does not digitize transmit pulse shapes, examining pulse shape differences over impenetrable targets (*e.g.,* airport runways) can be considered a proxy when examining 1064 nm and 532 nm return pulse characteristics. During the 2014 Alaska campaign, there were fifteen 532 nm beams and six 1064 nm beams. Our analysis used relatively high-energy beams. For analysis intended to mimic the 90 m spacing of the ATLAS beam geometry, two 1064 nm beams were chosen based on their across-track ground separation and along-track signal-photon density: beams 43 (center of the array) and 48 (~90 m to the left of the array center across-track). For analysis intended to assess issues that might be wavelength-dependent, beams 5 (532 nm) and 50 (1064 nm) were chosen because, in an along-track direction, they were in line with one another at approximately 35 m to the left of the array center in the across-track direction.

Each MABEL beam has a unique range bias. This is also the result of the unique optical path that each beam follows through the instrument. Much of the analysis performed here, such as evaluation of local surface slope, did not require absolute range accuracy.

The Cryosphere Discuss., doi:10.5194/tc-2015-225, 2016
Manuscript under review for journal The Cryosphere
Published: 19 January 2016

Therefore, the individual beams were generally only calibrated to one another based on data collected over the nearest flat surface (*e.g.*, open water). These calibrations were made relative to the beam closest to the center of the array.

2.2 MABEL camera imagery

For the 2014 Alaska campaign, a camera was integrated with MABEL and was successful for over 40% of the campaign's duration. The images were typically used to visually confirm the type of surface being measured by MABEL (*e.g.*, ice, open water, sea ice, or melt ponds) or to confirm the presence or absence of clouds. These images are also available on the ICESat-2 website. The MABEL camera is a Sony Nex7, with a 55 to 220 mm, f/4.5-6.6 telephoto lens. It was mounted on the same optical bench as the MABEL telescopes and shared the same portal in the aircraft. At a nominal aircraft altitude of 20 km, each image covers an approximately 2.25 by 1.5 km area. At the same altitude, MABEL beams for the Alaska campaign had a total swath width of approximately 200 m, and thus were wholly contained within the camera images. The images collected were not systematically georeferenced; however, they were time-stamped based on MABEL instrument timing to provide a first-order assessment of the surface that the lidar had surveyed.

2.3 Landsat 8 and WorldView-2 imagery

Data from the Landsat 8 Operational Land Imager (OLI) on the Bagley Icefield (Fig. 1b) were used as an independent assessment of the depths of melt ponds surveyed by MABEL. We applied spectrally based depth-retrieval models to Landsat 8 imagery (Moussavi, 2015; Pope et al., 2015; Moussavi et al., 2014), which were calibrated based on data from supraglacial lakes in Greenland. The models compare Landsat 8 spectral reflectance over the lakes during pre-drainage with a post-drainage digital elevation model (DEM), derived from WorldView-2 imagery acquired from the Polar Geospatial Center at the University of Minnesota, using image-processing software (ERDAS). Given

The Cryosphere Discuss., doi:10.5194/tc-2015-225, 2016
Manuscript under review for journal The Cryosphere
Published: 19 January 2016

the small size of the melt ponds on the Bagley Icefield, we used reflectance values recorded in the panchromatic channel of OLI imagery.

A second WorldView-2-derived DEM was used near the terminus of the Lower Taku Glacier (Fig. 1c) to assess surface elevations derived from MABEL signal photons in steep and crevassed terrain. The DEM, created by the Polar Geospatial Center at the University of Minnesota, was extracted from high-resolution along-track stereo WorldView-2 imagery processed with NASA's open source Ames Stereo Pipeline software (Moratto et al., 2010).

2.4 Juneau Icefield GPS data

Previous studies (Brunt et al., 2013; Brunt et al., 2014) have demonstrated that MABEL precisely characterizes the ice-sheet surface when comparing MABEL-derived slope on 90 m across-track length scales with those based on both Airborne Topographic Mapper (ATM; Krabill et al., 2002) and Laser Vegetation Imaging Sensor (LVIS, more recently referred to as Laser Vegetation Ice Sensor; Blair et al., 1999).

We designed a GPS survey on the Juneau Icefield (Fig. 1c) to determine the length-scale at which a ground-based local slope assessment on a flat surface (<1° slope) begins to differ significantly from that of the 90 m across-track slope assessment based on MABEL. On 19 July 2014, we conducted differential GPS surveys of the nodes of a series of concentric equilateral triangles. WGS84 ellipsoidal heights, in a Universal Transverse Mercator map projection (UTM zone 8N), were determined for each node using Trimble 5700 base and rover receivers, operating in real-time differential mode. The base-station receiver was located at the Juneau Icefield Research Program (JIRP) Camp 10, approximately 1 km from where the rover receivers were operated. Eight triangles were surveyed with side lengths of 5, 10, 25, 50, 75, 90, 125, and 150 m (Fig. 2, black points). We fit a surface to each of the eight triangles and then calculated the surface slope in both the UTM easting and northing directions (surface gradients $\delta z/\delta x$ and $\delta z/\delta y$).

The Cryosphere Discuss., doi:10.5194/tc-2015-225, 2016
Manuscript under review for journal The Cryosphere
Published: 19 January 2016

MABEL-based surface gradients $\delta z/\delta x$ and $\delta z/\delta y$ were generated from data from the 31 July 2014 flight and compared with the GPS-based surface gradients. We used beams 43 and 48 (1064 nm), which had relatively high along-track signal-photon density, approximately 90 m ground spacing, and intersected the GPS survey array (Fig. 2, red lines). The MABEL beams were cross-calibrated to remove the relative elevation bias resulting from their different optical paths through the instrument. To accomplish this calibration, we chose beam 43 as a reference beam, calculated the mean difference between the signal photons of the reference beam and beam 48 over the nearest open ocean, and removed that offset (0.2 m) from beam 48. We projected the geodetic MABEL data to the gridded map projection of the GPS data (UTM zone 8N) to facilitate direct comparisons and so that changes in elevation in both the easting and northing directions (surface gradients $\delta z/\delta x$ and $\delta z/\delta y$) could be treated uniformly. We generated a MABEL triangle, with nodes based on the intersections of the GPS survey and the ground tracks of the MABEL beams (Fig. 2, blue solid points). We then fit a surface to those points and calculated the associated MABEL surface gradient in both the easting and northing directions ($\delta z/\delta x$ and $\delta z/\delta y$). Based on this surface, the local slope for the survey area was 0.5°, or comparable to what we expect for an ice-sheet interior. Finally, we generated a surface based on the three GPS survey sites that were closest to the nodes that defined the MABEL surface (Fig. 2, blue open circles).

We compared the MABEL-derived slopes to the slopes from each of the concentric GPS triangles and the slope based on the GPS survey sites that were closest to the nodes that defined the MABEL surface. Specifically, we created a surface gradient comparison (SGC) parameter for each of the GPS-derived triangles (i) by calculating the square root of the sum of the squares (RSS) of the differences between the MABEL-derived and GPS-derived slopes in both the easting and northing (x and y) directions:

$$SGC_{(i)} = \sqrt{\left[(\delta z/\delta x)_{MABEL} - (\delta z/\delta x)_{GPS_{(i)}}\right]^2 + \left[(\delta z/\delta y)_{MABEL} - (\delta z/\delta y)_{GPS_{(i)}}\right]^2}, \quad (1)$$

where $\delta z/\delta x$ and $\delta z/\delta y$ are the surface gradients associated with both MABEL and each of the GPS triangles (i), in the easting and northing directions.

The Cryosphere Discuss., doi:10.5194/tc-2015-225, 2016
Manuscript under review for journal The Cryosphere
Published: 19 January 2016

2.4 Lower Taku Glacier GPS data

The WorldView-2 images used to construct the Lower Taku Glacier DEM were collected on 6 June 2014, while the MABEL data were collected on 16 July 2014 and thus, separated by 40 days. GPS data were collected at six sites on the Lower Taku Glacier throughout the summer, using a Trimble NetR9 receiver and used to tie the MABEL survey data to the WorldView-2 DEM. The data were processed kinematically using the Plate Boundary Observatory station AB50, located at the Mendenhall Glacier Visitor Center, approximately 20 km west of the survey area. Velocities based on the GPS data were used to migrate the MABEL data to match the timing of the WorldView-2 image acquisition.

3 Results

3.1 MABEL signal-photon density

For illustrative purposes, we produced histograms of the MABEL surface-return for the beams used in our analyses (Fig. 3; beams 5, 43, 48, and 50) from 3000 m of along-track data over a stretch of open ocean. We calibrated the beam elevations to one another to remove the unique beam elevation biases, and then detrended the surface elevations based on a linear fit to the signal photons to remove any elevation differences associated with wind stress or ocean dynamic topography. We then produced histograms for the entire 3000 m of open ocean surface-return data using a 1 cm vertical bin size. We determined the full width at half maximum (FWHM) for each of the beams, which ranged from 0.19 m in beam 5 (532 nm) to 0.31 m in beam 43 (1064 nm). From Fig. 3, the relative differences in the signal strengths of the individual beams are evident in the non-uniform amplitudes of the photon-count distribution.

The MABEL return signal often demonstrates a strong surface return and a second, weaker return approximately 0.5 to 1.5 m below the surface. This is due to unintended secondary pulses from the MABEL laser that occur under some operational conditions. These instrumental issues are more noticeable in the 1064 nm beams, but are minimized when the 1064 nm source is frequency-doubled to generate 532 nm beams. This second

The Cryosphere Discuss., doi:10.5194/tc-2015-225, 2016
Manuscript under review for journal The Cryosphere
Published: 19 January 2016

pulse can affect statistics associated with MABEL results and was therefore generally removed. This secondary pulse is evident in the open-ocean data example at approximately 0.75 m below the main surface return (Fig. 3).

Given nearly uniform surface conditions, along-track signal-photon density for each beam varied within and between flights based on parameters such as reflectivity, weather conditions, time of day, and sun-incidence angle. The signal-photon densities on the Juneau and Bagley icefields, for each beam considered here, are given in Table 1. These densities are reported based on 70 cm along-track length scales for direct comparison with previous results (Brunt et al., 2014), to mimic the ATLAS sampling interval (one laser shot every 70 cm), and for direct comparison with ATLAS performance models. MABEL along-track signal-photon densities for the July 2014 Alaska campaign were lower than those reported during the April 2012 Greenland campaign by Brunt et al. (2014); they reported 3.4 and 3.9 signal photons per 70 cm for beams 5 and 6 (532 nm), respectively. Some of this variation may have been related to seasonal differences in surface reflectivity between the two campaigns, which include parameters such as sun angle, the freshness of the most recent snowfall, the dust content of the surface, the presence (or absence) of surface melt and ponds, and the presence (or absence) of snow bridges that cover crevasses. Some variation may also have been related to instrumentation issues, such as cleanliness of the elements in the optics.

The MABEL signal-photon densities (Table 1) are less than that expected for ATLAS. Under similar conditions as the 2014 MABEL summer campaign, based on performance models, we expect the strong beams of ATLAS to record 8.5 signal photons every shot (or 70 cm along track) over ice sheets and 2.0 signal photons every shot over the open ocean (A. Martino, NASA GSFC, personal communication 2014). We note that for the Alaskan icefields, the expected number of signal photons based on the performance model is high, as the model uses an albedo of 0.9, which is more appropriate for ice with fresh snow or the interior of Antarctica. Relative to the performance model, the MABEL data used in this analysis suggest that the signal-photon densities were ~65% of the expected ATLAS signal-photon densities over open ocean and ~44% of the expected ATLAS signal-photon densities over summer ice sheets. For ICESat-2 development

The Cryosphere Discuss., doi:10.5194/tc-2015-225, 2016
Manuscript under review for journal The Cryosphere
Published: 19 January 2016

purposes, efforts are underway to merge data from adjacent MABEL beams, which will facilitate more direct MABEL to ATLAS comparisons.

3.2 Elevation bias and uncertainty

We compared MABEL elevations to those based on the Juneau Icefield GPS array, interpolated to the MABEL/GPS points of intersection (Fig. 2, blue solid points). The mean offset, or bias, for the three points of intersection was 3.2 ±0.08 m. While this 3 m instrument bias is larger than that of other airborne lidars, it is within the MABEL design goals (algorithm development, error analysis, and ATLAS model validation), where instrument precision is more critical to satellite algorithm development than absolute accuracy. Thus, while other photon-counting systems are being used for change detection (*e.g.*, Young et al., 2015), in its current configuration, MABEL is not suitable for time-series analysis of elevation change, either independently or when integrated with other datasets.

We assessed the surface precision of MABEL data (*i.e.*, the spread of the MABEL data point cloud about a known surface, or the standard deviation of the mean difference between MABEL and a known surface elevation, Hodgson, and Bresnahan, 2004) over a flat stretch of open ocean. For approximately 3000 m of along-track open water, the surface-precision estimates for the strong 532 and 1064 nm beams, based on a standard deviations of the mean differences from the flat surface, were ±0.11 and ±0.12 m, respectively. Brunt et al. (2014) reported similar surface-precision values (±0.14 m) based on direct comparison of MABEL elevation data with high-resolution ground-based GPS data (differentially post-processed with an RMS < 5 cm) over an airport departure apron. Further, Brunt et al. (2013) reported that for all MABEL campaigns (2010 – 2014), when similar ground-based GPS data were available, MABEL surface precision ranged between ±0.11 and ±0.24 m. During that time period, MABEL had been deployed on two different types of aircraft and in a number of different optical configurations (McGill et al., 2013).

The Cryosphere Discuss., doi:10.5194/tc-2015-225, 2016
Manuscript under review for journal The Cryosphere
Published: 19 January 2016

3.3 Local slope assessment for ice-sheet interiors

Using Eq. (1), we compared the MABEL-derived surface-gradient comparison (SGC) parameters to those based on the Juneau Icefield GPS array (Fig. 4). The MABEL-derived SGC parameters were consistent with GPS-derived SGC parameters over length scales ranging from 50 m (just over half of the ATLAS beam spacing) to 150 m (just under twice the ATLAS beam spacing). The SGCs for 50 to 150 m spatial scales were less than 0.2°.

3.4 Surface characterization

Analysis of data from individual beams over the Bagley Icefield indicated that MABEL can capture surface detail of crevasse fields. Fig. 5a shows stitched MABEL images of one set of crevasses on the Bagley Icefield; Fig. 5b shows MABEL signal and background photons for a 500 m range that includes the glacier surface; and Fig. 5c shows MABEL signal photons, indicating both the glacier surface and the bottoms of a series of crevasses. The along-track slope of this crevasse field, between 140.60° and 140.56° W longitude in Fig. 5c, is 1°.

Similarly, analysis of the individual beams on a different stretch of the Bagley Icefield indicated that MABEL can determine the location of melt ponds. Fig. 6a shows stitched MABEL images from crevasse and melt-pond fields on the Bagley Icefield; Fig. 6b shows MABEL signal and background photons for a 500 m range window that includes the glacier surface; Fig. 6c shows both signal and background photon-count densities (per 125 shots, or ~2.5 m of along-track distance); and Fig. 6d shows MABEL signal photons, indicating the location of a melt pond, which is approximately 70 m in along-track length. The along-track slope of this crevasse field, between 141.90° and 141.86° W longitude in Fig. 6d, is 2°. A histogram of the signal photons associated with the location of the melt pond in the inset of Fig. 6d is provided in Fig. 7. This was generated to investigate how the penetration of light into the melt pond, at 532 and 1064 nm wavelengths, would affect the statistics of the return signal. The FWHM for the 532 and 1064 nm return signal were 0.26 and 0.34 m, respectively. We applied spectrally based depth-retrieval models to Landsat 8 imagery (Moussavi, 2015; Pope et al., 2015; Moussavi et al., 2014) for an

The Cryosphere Discuss., doi:10.5194/tc-2015-225, 2016
Manuscript under review for journal The Cryosphere
Published: 19 January 2016

independent assessment of the depth of the melt-pond on the Bagley Icefield in Fig. 6d. This analysis indicated that melt ponds in this region were approximately 2 m deep.

Analysis of data from individual beams near the terminus of the Lower Taku Glacier (Fig. 8) provided insight in to how MABEL will operate in regions of steeper slope. The slope in this region is 4° and more consistent with slopes on an ice-sheet margin. A slope of 4° is also the maximum angle used for ATLAS performance modeling over ice-sheet margins (A. Martino, NASA GSFC, personal communication 2014). Fig. 8a shows stitched MABEL camera images, which suggest a much rougher surface than that of the low slope areas of interest on the Bagley Icefield examined in Fig. 6. Additionally, the MABEL ice-surface signal near the terminus was slightly compromised due to intermittent cloud cover, which attenuated the MABEL transmit laser pulses. Further, when cloud cover allows for only intermittent surface determination, the surface-finding algorithm used to discriminate signal photons from background and noise photons is compromised.

MABEL-derived surface elevations over the Lower Taku Glacier were compared to elevations from the WorldView-2-derived DEM (Fig. 8b), which had 2 m horizontal-resolution. Fig. 8c is one of the images used to create the DEM shown in Fig. 8d. GPS data collected on the Lower Taku Glacier were used to determine an ice-flow velocity of 0.2 m day^{-1} at SDWN (Fig. 8c, 800 m from the center of the MABEL data line). Ice-flow velocities for the two central GPS sites (Fig. 8c, C10 and SLFT, 1500 m from the center of the MABEL data line) were 0.7 m day^{-1}, while velocities for the three northern GPS sites (Fig. 8c, C20, SRIT, and SUP, 3000 m from the center of the MABEL data line) were 1.0 m day^{-1}. The northing and easting components of the SDWN velocity were used to migrate the MABEL data to match the timing of the WorldView-2 image acquisition. An elevation was then extracted from the WorldView-2 DEM for each migrated MABEL data point. The MABEL elevations, or the red points in Fig. 8b, were corrected for a range bias and migrated based on the velocities of SDWN for direct comparison with the elevation values extracted from the WorldView-2 DEM, or the black points in Fig. 8b. While SDWN is not ideal for the entire MABEL data line, we chose this GPS site based on proximity to the center of the data line and because the direction of flow in the northing and easting directions matched the southern end of the MABEL data line.

The Cryosphere Discuss., doi:10.5194/tc-2015-225, 2016
Manuscript under review for journal The Cryosphere
Published: 19 January 2016

MABEL elevations were 8 m lower than the values extracted from the WorldView-2 DEM. This bias is higher than other biases assessed during this campaign. We attribute the difference to: 1) the difference between the DEM and true elevation, which can be on the order of meters to 10 meters; 2) a standard MABEL range bias, which is approximately 3 m; and 3) the amount of surface melting that occurred between June and July, which is approximately 3 m.

Migration of the MABEL data to take into account ice flow had a very small effect on the MABEL surface-elevation statistics, relative to the WorldView-2 DEM. This is probably due to the orientation of the MABEL survey line, which was oblique to the ice-flow lines. Further, we note that elevation uncertainty is a function of MABEL horizontal uncertainty (2 m) and surface slope; therefore, steeper terrain leads to greater overall elevation uncertainty (Brunt et al., 2014). While the MABEL surface precision (*i.e.*, the standard deviation of the mean difference between the MABEL and DEM elevations) of all of the Lower Taku Glacier data in Fig. 8b was slightly lower after the migration of the data (from 2.6 m to 2.5 m, for beam 43), the surface precision was appreciably lower (1.8 m) when comparing only the southern part of the data line (<58.43° latitude), where the data were more consistent with the ice-flow lines and were closer to the GPS site used in this analysis (Fig. 8c, SDWN). Unfortunately, the southernmost section of the data line was slightly compromised by intermittent cloud cover.

3.5 Slope assessment for steeper glacial settings

The high-resolution WorldView-2 DEM also provided a means of assessing MABEL-derived across-track slopes in steeper glacial settings. Similar to the methods of Brunt et al. (2014), we calculated a ~40 m across-track MABEL-derived slope and compared this with a ~40 m across-track slope based on WorldView-2 DEM elevations. The MABEL-derived across-track slope was calculated using beams 43 and 50, migrated to match the timing of the WorldView-2 image acquisition and limited to continuous stretches of the southern part of the data line. Along-track signal-photon density for beam 48 was insufficient to allow for a 90 m across-track assessment. The MABEL data from each beam were interpolated along track to a common time so that along-track elevations for

The Cryosphere Discuss., doi:10.5194/tc-2015-225, 2016
Manuscript under review for journal The Cryosphere
Published: 19 January 2016

each beam could be used to calculate an across-track slope for each increment of along-track time. A DEM-derived across-track slope was calculated based on elevations that were extracted from the DEM at each migrated MABEL data point for beams 43 and 50. Fig. 9a shows good agreement between the MABEL and DEM elevations associated with beam 43. Similarly, Fig. 9b shows good agreement between MABEL-derived and DEM-derived across-track slopes. The total along-track distance used in this analysis was ~300 m (see box in Fig. 8b). The mean residual between the MABEL-derived slope and the DEM-derived slope was 0.25°.

4 Discussion

The result of this analysis indicates that the MABEL-derived local slope assessment, on a relatively flat glacial surface and on a 90 m across-track length scale, is consistent with *in situ* slope assessments made at spatial scales ranging from 50 to 150 m. For a planar surface, such as the interior of an ice sheet, where slope is less than 1°, we expect the local slope measured by a GPS survey and MABEL to be similar, over a wide range of spatial scales. Any small differences observed between the two survey techniques would likely reflect 1) the non-planarity of the surface and/or 2) the sensitivity of the results to small-scale slopes or roughness captured by one measurement technique and not the other. With the good observed agreement between MABEL-derived and GPS-derived slope assessments over 50 to 150 m length scales (Fig. 4), we feel confident that the ATLAS 90 m beam-spacing strategy will provide a robust estimate of local slope for ice-sheet interiors (<1°) over a wide range (50 to 150 m) of spatial scales. This knowledge is necessary for accurate assessments of ice-sheet surface-elevation change.

Figs. 5c and 6d suggest that the dense along-track sampling of MABEL is sufficient to provide surface detail, including melt-pond information, from a single, static beam in regions of low slope, consistent with that of an ice-sheet interior. Based on the continuous nature of the surface return through the crevasse field, especially in the 1064 nm beam (50) in Fig. 5c, we conclude that MABEL is generally retrieving a signal from the bottom of the crevasses. Further, Fig. 8b indicates that MABEL continues to provide surface detail in regions of steeper slope, including the retrieval of the steep slopes of the

The Cryosphere Discuss., doi:10.5194/tc-2015-225, 2016
Manuscript under review for journal The Cryosphere
Published: 19 January 2016

crevasse walls (*e.g.*, Figs 5c and 6d). As previously noted, MABEL data used in this analysis had signal-photon densities are ~44% of the expected ATLAS signal-photon densities over summer ice sheets (A. Martino, NASA GSFC, personal communication 2014). Therefore, we believe that the detail of ATLAS will be sufficient to determine local surface characteristics, similar to those observed on the Lower Taku Glacier. Such knowledge is critical to determining ice-sheet surface-elevation change, as features that could compromise change calculations, such as deep crevasses, can move or advect with ice-sheet flow.

The crevasse characterization associated with the Bagley Icefield is qualitatively confirmed using the camera imagery (Fig. 5a). However, it should be noted that we have no means of quantitatively assessing the accuracy of MABEL-derived crevasse depths. Crevasses on an ice-sheet surface have an influence on solar radiation and albedo (Pfeffer and Bretherton, 1987). This variation in reflectance is evident in Figs. 5b, 6b, and 6c, where MABEL background photon counts, and the signal-to-noise ratios, change significantly. Changes in MABEL background photon densities have also been used to detect leads in sea ice (Kwok et al., 2014; Farrell et al., 2015). From Fig. 6c we note that the overall background photon counts decrease significantly over the eastern region of this plot, which is characterized by crevasses. However, this change is non-uniform. Background photon counts drop steadily to nearly zero over the two melt ponds surveyed along this transect.

The surface characterization of the Lower Taku Glacier is assessed using the camera imagery, WorldView-2 imagery, and a DEM derived from the WorldView-2 imagery (Fig. 8). Once the MABEL data have been migrated based on GPS ice-flow velocities, the southern part of the MABEL-derived surface elevations are in good agreement with the DEM data. However, the MABEL signal in this section is intermittent due to cloud cover. In the northern part of the MABEL data line, while the migration failed to improve surface-elevation statistics, a generally continuous signal is detected, including melt ponds (Fig. 8b, inset). The slope comparison between MABEL-derived across-track slope and DEM-derived across-track slope had a mean residual of 0.25°. This residual is larger than that reported over the Greenland Ice Sheet (<0.05°) by Brunt et al. (2014); we attribute this difference to errors associated with the migration of the MABEL data, given

The Cryosphere Discuss., doi:10.5194/tc-2015-225, 2016
Manuscript under review for journal The Cryosphere
Published: 19 January 2016

that the flight line was oblique to the local direction of ice flow. Since the GPS array on the Lower Taku Glacier was not optimized to facilitate an across-track slope comparison similar to the comparison made higher up on the Juneau Icefield (Figs. 2 and 4), we do not expect good agreement between the two methods of estimating across-track slope.

Penetration of 532 nm wavelength light into the surface, be it a melt pond or snow, is an ongoing area of research for ICESat-2 algorithm development. Based on the signal-photon elevations in the inset in Fig. 6d, and the histogram of the signal photons in Fig. 7, the total spread of the signal photons, at a wavelength of 532 nm, is approximately 1.5 to 2 m. Further, analysis of Landsat 8 and WorldView-2 imagery confirm that the melt ponds in this region are approximately 2 m deep. These results suggest that the 532 nm MABEL beam may be sampling the entire melt-pond water column. The 1064 nm MABEL beam shows evidence of a secondary return 1.5 m below the main signal return, due to unintended secondary pulses from the MABEL laser that occur under some operational conditions.

Based on the surface characterization results of MABEL data from the Juneau and Bagley icefields, and the dense, six-beam sampling strategy of ATLAS, we feel confident that ICESat-2 will contribute significantly to glacier studies at local and regional scales and in polar and mid-latitudes. While previous studies using satellite laser altimetry have investigated the vertical dimension of rifts in the ice sheet (*e.g.*, Fricker et al., 2005), those studies have been limited to major ice-shelf rift systems, as opposed to smaller-scale crevasses. The 70 cm along-track sampling density of each individual ATLAS beam is well suited for similar vertical dimension studies, but at finer length-scales, such as those associated with alpine glacier crevasse fields.

5 Conclusions

Knowledge of local slope and local surface character are required to accurately determine ice-sheet surface-elevation change. ATLAS beam geometry includes pairs of beams separated at 90 m across track to enable the determination of local slope in one pass and, therefore, to enable the determination of ice-sheet surface-elevation change in just two passes. Based on the analysis of MABEL and ground-based GPS data, and the resultant

The Cryosphere Discuss., doi:10.5194/tc-2015-225, 2016
Manuscript under review for journal The Cryosphere
Published: 19 January 2016

surface gradient comparison (SGC), we conclude that the ATLAS 90 m beam-spacing strategy will provide a robust assessment of local slope that is consistent with the slope of an ice-sheet interior (<1°) on 50 to 150 m length scales. The density of along-track photon-counting lidar data is sufficient to characterize the ice-sheet surface in detail, including small-scale features such as crevasses and melt ponds. This information is also required for accurate determination of ice-sheet surface-elevation change.

The MABEL 2014 Alaska campaign was timed to collect data during the summer melt season to specifically investigate how 532 nm wavelength laser light interacts with a melting snow surface. Results from MABEL, and confirmed through analysis of Landsat 8 imagery, suggest that 532 nm wavelength light is likely reflecting from the surface and subsurface of the 2 m deep supraglacial melt ponds on the Bagley Icefield. This is an ongoing area of research for ATLAS and ICESat-2 algorithm development.

Acknowledgements

Funding for this project was through the NASA ICESat-2 Project Science Office. Funding for J.M. Amundson was provided by NSF-PLR 1303895. We acknowledge the considerable efforts of the Project, Science, and Instrument teams of NASA's ICESat-2 and MABEL missions. We thank: Eugenia De Marco (ASRC Aerospace Corp., NASA/GSFC) and Dan Reed (Sigma Space Corp., NASA/GSFC) for MABEL instrument support; Scott Luthcke (NASA/GSFC), David Hancock (NASA/WFF), and Jeff Lee (NASA/WFF) for MABEL data calibration; Scott McGee and Ya' Shonti Bridgers (JIRP) for GPS field data collection and data processing support; and NASA/AFRC (specifically ER-2 pilots Tim Williams and Denis Steele) for Alaska airborne support. WorldView imagery was provided by the Polar Geospatial Center at the University of Minnesota, which is supported by NSF-PLR 1043681. GPS receivers for the survey of the terminus of the Lower Taku Glacier were provided by UNAVCO. GPS receivers for the JIRP survey were provided by Werner Stempfhuber of the Beuth Hochschule for Technik University of Applied Sciences.

The Cryosphere Discuss., doi:10.5194/tc-2015-225, 2016
Manuscript under review for journal The Cryosphere
Published: 19 January 2016

References

Abdalati, W., Zwally, H., Bindschadler, R., Csatho, B., Farrell, S., Fricker, H., Harding, D., Kwok, R., Lefsky, M., Markus, T., Marshak, A., Neumann, T., Palm, S., Schutz, B., Smith, B., Spinhirne, J., and Webb, C.: The ICESat-2 laser altimetry mission, Proc. IEEE, 98, 735–751, doi: 10.1109/JPROC.2009.2034765, 2010.

Blair, J., Rabine, D., and Hofton, M., The Laser Vegetation Imaging Sensor: a medium-altitude, digitisation-only, airborne laser altimeter for mapping vegetation and topography, ISPRS Journal of Photogrammetry and Remote Sensing, 54, 115–122, doi: 10.1016/S0924-2716(99)00002-7, 1999.

Brunt, K., Neumann, T., Walsh, K., and Markus, T.: Determination of local slope on the Greenland Ice Sheet using a multibeam photon-counting lidar in preparation for the ICESat-2 mission, IEEE Geoscience and Remote Sensing Letters, 11, 935–939, doi: 10.1109/LGRS.2013.2282217, 2014.

Brunt, K., Neumann, T., Markus, T., and Walsh, K.: MABEL photon-counting laser altimetry data for ICESat-2 simulations and development, AGU Fall Meeting, San Francisco, CA, Dec. 2013.

Farrell, S., Brunt, K., Ruth, J., Kuhn, J., Connor, L., and Walsh, K.: Sea ice freeboard retrieval using digital photon-counting laser altimetry, Annals of Glaciology, 56, 167–174, doi: 10.3189/2015AoG69A686, 2014.

Fricker, H., Bassis, J., Minster, B., and MacAyeal, D.: ICESat's new perspective on ice shelf rifts: The vertical dimension, Geophysical Research Letters, 32, doi: 10.1029/2005GL025070, 2005.

Hodgson, M., and Bresnahan, P.: Accuracy of airborne lidar-derived elevation: empirical assessment and error budget, Photogramm. Eng. Remote. Sens., 70, 331–340, doi: 10.14358/PERS.70.3.331, 2004.

Krabill, W., Abdalati, W., Frederick, E., Manizade, S., Martin, C., Sonntag, J., Swift, R., Thomas, R., and Yungel, J.: Aircraft laser altimetry measurement of elevation changes of the Greenland ice sheet: Technique and accuracy assessment, J. Geodyn., 34, 357–376, doi: 10.1016/S0264-3707(02)00040-6, 2002.

Kwok, R., Cunningham, G., Manizade, S., and Krabill, W.: Arctic sea ice freeboard from IceBridge acquisitions in 2009: Estimates and comparisons with ICESat, J. Geophys. Res., 117, C02018, doi: 10.1029/2011JC007654, 2012.

Martino, A., NASA Goddard Space Flight Center, personal communication, 2014.

McGill, M., Markus, T., Scott, V., and Neumann, T.: The Multiple Altimeter Beam Experimental Lidar (MABEL), an airborne simulator for the ICESat-2 mission, J. Atmos. Oceanic Technol., 30, 345–352, doi: 10.1175/JTECH-D-12-00076.1, 2013.

Moratto, Z, Broxton, M., Beyer, R., Lundy, M., and Husmann, K. (2010), Ames Stereo Pipeline, NASA's Open Source Automated Stereogrammetry Software, presented at the Lunar and Planetary Science Conference, Houston, Texas.

Moussavi, M.: Quantifying supraglacial lake volumes on the Greenland ice sheet from spaceborne optical sensors (2015). Thesis (Ph.D.) University of Colorado at Boulder; AAT 3704777; ISBN: 9781321773804; Dissertation Abstracts International, Volume: 76-10(E), Section: B.; 128 p.

Moussavi, M., Abdalati, W., Pope, A., and Scambos, T.: Validation of Supraglacial lake bathymetry models developed for optical sensors using high-resolution stereo-imagery, AGU Fall Meeting, San Francisco, CA, Dec, 2014.

Pfeffer, W., and Bretherton, C.: The effect of crevasses on the solar heating of a glacier surface, The Physical Basis of Ice Sheet Modelling, IAHS Publication 170, 191–205, 1987.

Pope, A., Scambos, T., Moussavi, M., Tedesco, M., Willis, M., Shean, D., and Grigsby, S.: Estimating supraglacial lake depth in western Greenland using Landsat 8 and comparison with other multispectral methods, The Cryosphere Discuss, 9, 3257–3292, doi: 10.5194/tcd-9-3257-2015, 2015.

Young, D., Lindzey, L., Blankenship, D., Greenbaum, J., De Gorordo, A., Kempf, S., Roberts, J., Warner, R., Van Ommen, T., Siegert, M., and Le Meur, E.: Land-ice elevation changes from photon-counting swath altimetry: first applications over the Antarctic ice sheet, J. Glaciol., 61, 17–28, doi: 10.3189/2015JoG14J048, 2015.

The Cryosphere Discuss., doi:10.5194/tc-2015-225, 2016
Manuscript under review for journal The Cryosphere
Published: 19 January 2016

1 Zwally, H., Li, J., Brenner, A., Beckley, M., Cornejo, H., DiMarzio, J., Giovinetto, M.,
2 Neumann, T., Robbins, J., Saba, J., Yi, D., and Wang, W.: Greenland ice sheet mass
3 balance: distribution of increased mass loss with climate warming; 2003-07 versus 1992-
4 2002, J. Glaciol., 57, 88–102, doi: 10.3189/002214311795306682, 2011.
5

The Cryosphere Discuss., doi:10.5194/tc-2015-225, 2016
Manuscript under review for journal The Cryosphere
Published: 19 January 2016

1 **Table 1.** MABEL along-track signal photon densities over the open ocean and the Juneau
2 and Bagley icefields.

	MABEL surface-signal photons per 70 cm		
Beam	open ocean	Juneau Icefield	Bagley Icefield
5 (532 nm)	0.3	1.8	1.7
43 (1064 nm)	1.2	3.5	2.8
48 (1064 nm)	0.5	1.5	1.0
50 (1064 nm)	1.3	3.7	3.0

3

The Cryosphere Discuss., doi:10.5194/tc-2015-225, 2016
Manuscript under review for journal The Cryosphere
Published: 19 January 2016

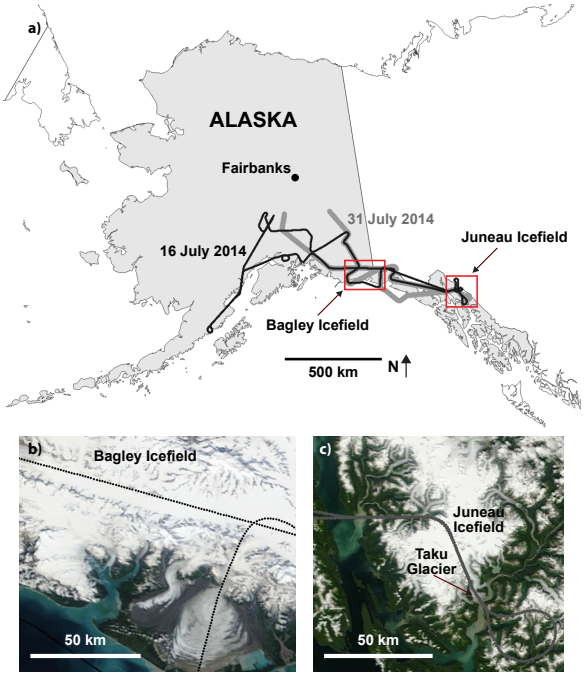

Figure 1. Map of the Multiple Altimeter Beam Experimental Lidar (MABEL) flights used in this analysis from the July 2014 field campaign, which was based out of Fort Wainwright, Fairbanks, Alaska. **(a)** Overview map, indicating the 16 and 31 July 2014 flight paths. **(b)** Inset of the Bagley Icefield, showing the 16 July 2014 flight path. **(c)** Inset of the Juneau Icefield, showing the 31 July 2014 flight path and the Taku Glacier. Both insets are shown with 31 July 2104 MODIS imagery.

The Cryosphere Discuss., doi:10.5194/tc-2015-225, 2016
Manuscript under review for journal The Cryosphere
Published: 19 January 2016

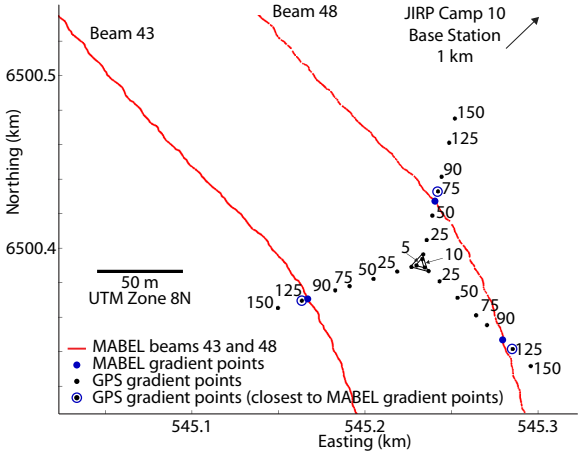

Figure 2. GPS survey on the Juneau Icefield. Ground tracks for MABEL beams 43 and 48, from the 31 July 2014 flight, are indicated (red lines). GPS survey points of the nodes of concentric, equilateral triangles, with side lengths of 5, 10, 25, 50, 75, 90, 125, and 150 m, are indicated (black points). Also indicated are the intersections of the MABEL flight lines with the GPS survey grid (blue solid points), which were used to calculate MABEL surface gradients ($\delta z/\delta x$ and $\delta z/\delta y$). The GPS sites that are the closest to the MABEL gradient points are also indicated (blue open circles). The overall slope, based on the MABEL elevations at the points of intersections with the GPS survey grid (blue solid points), is approximately 0.5°.

The Cryosphere Discuss., doi:10.5194/tc-2015-225, 2016
Manuscript under review for journal The Cryosphere
Published: 19 January 2016

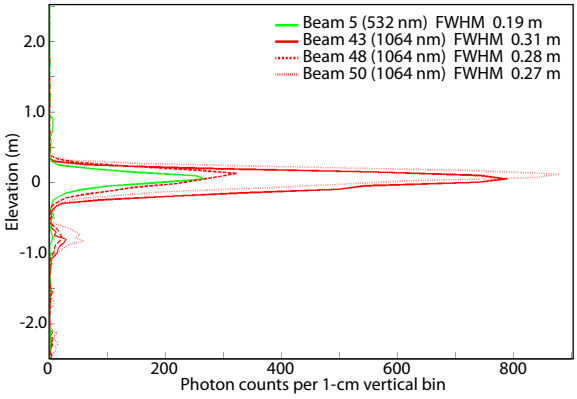

Figure 3. Histograms of the signal return for the MABEL beams used in this analysis (5, 43, 48, and 50). Plotted are ocean surface-return photon counts (per 1 cm vertical bins) over a 3 km along-track distance against elevation (m). The elevations are calibrated to one another and detrended. The full width at half maximum (FWHM) for each histogram are indicated in the legend. The secondary return 0.75 m below the main signal return, which is more evident in the 1064 nm beams, is due to unintended secondary pulses from the MABEL laser that occur under some operational conditions; this was removed for FWHM analysis.

The Cryosphere Discuss., doi:10.5194/tc-2015-225, 2016
Manuscript under review for journal The Cryosphere
Published: 19 January 2016

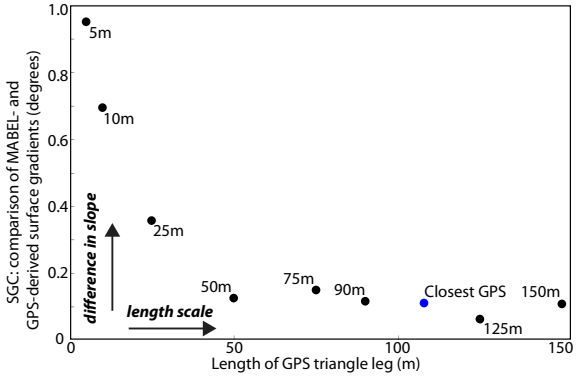

Figure 4. A surface-gradient comparison between a MABEL-derived surface (blue points in Fig. 2) and a series of GPS-derived surfaces, based on concentric equilateral triangles (black points here and in Fig. 2) and a surface based on the GPS survey sites that were closest to the nodes that defined the MABEL surface (blue point here and blue open circles in Fig. 2). The x-axis is the length of each side of the equilateral triangles (or a mean length, for the 'Closest GPS' surface); the y-axis is the surface-gradient comparison (SGC) parameter (defined in Eq. 1), or the RSS of the difference in surface gradient ($\delta z/\delta x$ and $\delta z/\delta y$), in degrees, between the MABEL-derived surface and each of the GPS-derived surfaces.

The Cryosphere Discuss., doi:10.5194/tc-2015-225, 2016
Manuscript under review for journal The Cryosphere
Published: 19 January 2016

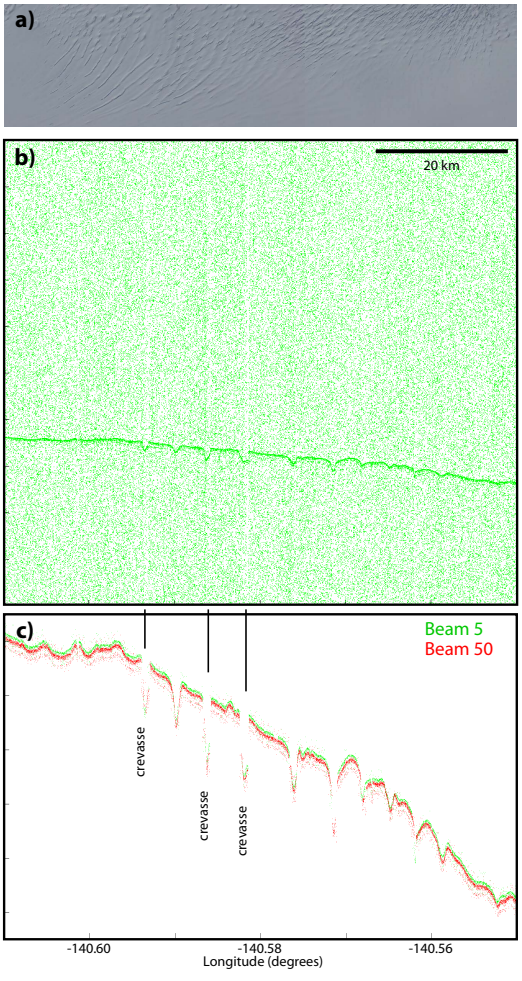

Figure 5. MABEL camera and photon data over a heavily crevassed section of the Bagley Icefield, from the 16 July 2014 flight. **(a)** Stitched MABEL camera images. **(b)** MABEL signal and background photons for a 500 m range that includes the glacier surface. **(c)** MABEL signal photons, indicating both the surface and the bottoms of crevasses. The along-track slope of this field, between 140.60° and 140.56° W longitude is 1°.

The Cryosphere Discuss., doi:10.5194/tc-2015-225, 2016
Manuscript under review for journal The Cryosphere
Published: 19 January 2016

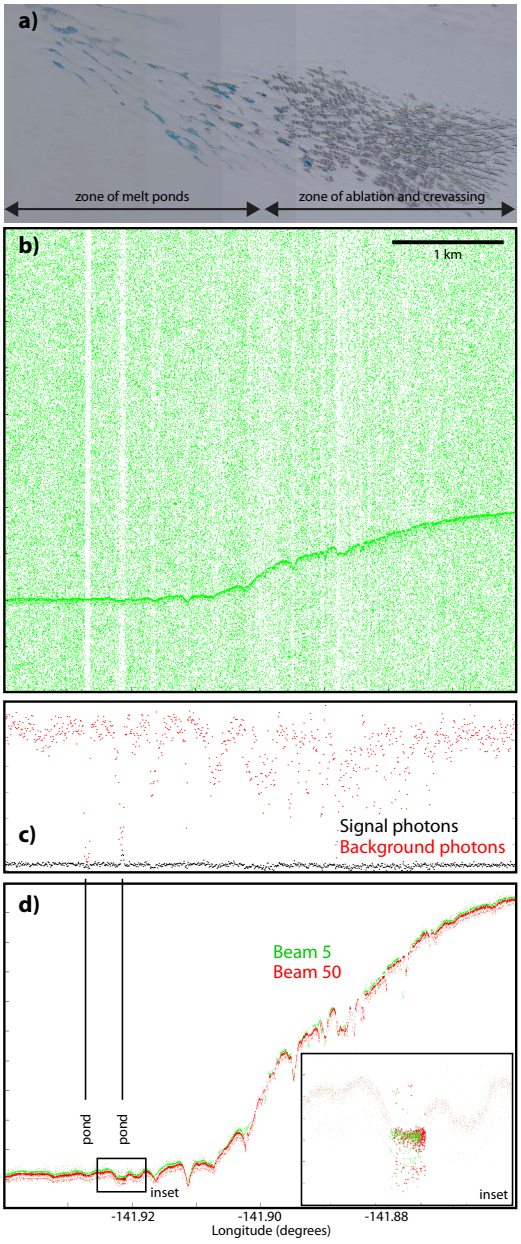

Figure 6. MABEL camera and photon data over crevasse and melt-pond fields on the Bagley Icefield, from the 16 July 2014 flight. **(a)** Stitched MABEL camera images. **(b)** MABEL signal and background photons for a 500 m range that includes the glacier

The Cryosphere Discuss., doi:10.5194/tc-2015-225, 2016
Manuscript under review for journal The Cryosphere
Published: 19 January 2016

surface. **(c)** Signal (black) and background (red) photon counts per 125 shots (approximately 2.5 m of along-track distance). **(d)** MABEL signal photons, indicating the location of melt ponds; the inset is a detail of one of the ponds, which is approximately 70 m in along-track length. The 1064 nm beam shows evidence of a secondary return 1.5 m below the main signal return, due to unintended secondary pulses from the MABEL laser that occur under some operational conditions. The along-track slope of the crevasse field, between 141.90° and 141.86° W longitude is 2°.

The Cryosphere Discuss., doi:10.5194/tc-2015-225, 2016
Manuscript under review for journal The Cryosphere
Published: 19 January 2016

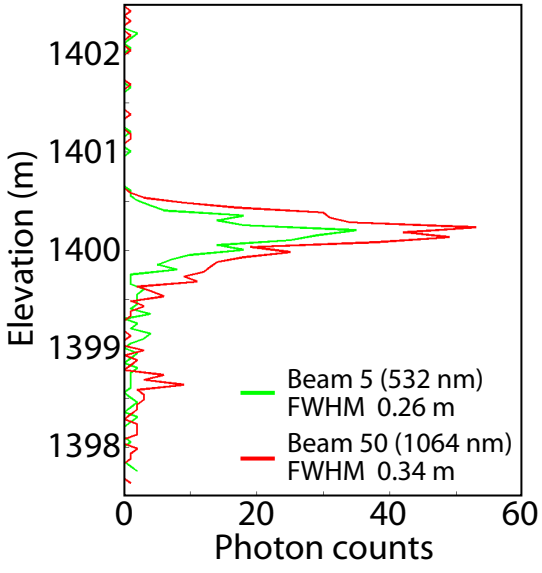

Figure 7. Histogram of the signal return for MABEL beams 5 (532 nm) and 50 (1064 nm) over the melt pond in Fig. 6. Plotted for each beam are surface-return photon counts per 1 cm vertical bins against elevation (m). The elevations of beams 5 and 50 are calibrated to one another. The full width at half maximum (FWHM) for each histogram are indicated in the legend. The secondary return <1 m below the main signal return, which is more evident in the 1064 nm beam, is due to unintended secondary pulses from the MABEL laser that occur under some operational conditions; this was removed for FWHM analysis.

The Cryosphere Discuss., doi:10.5194/tc-2015-225, 2016
Manuscript under review for journal The Cryosphere
Published: 19 January 2016

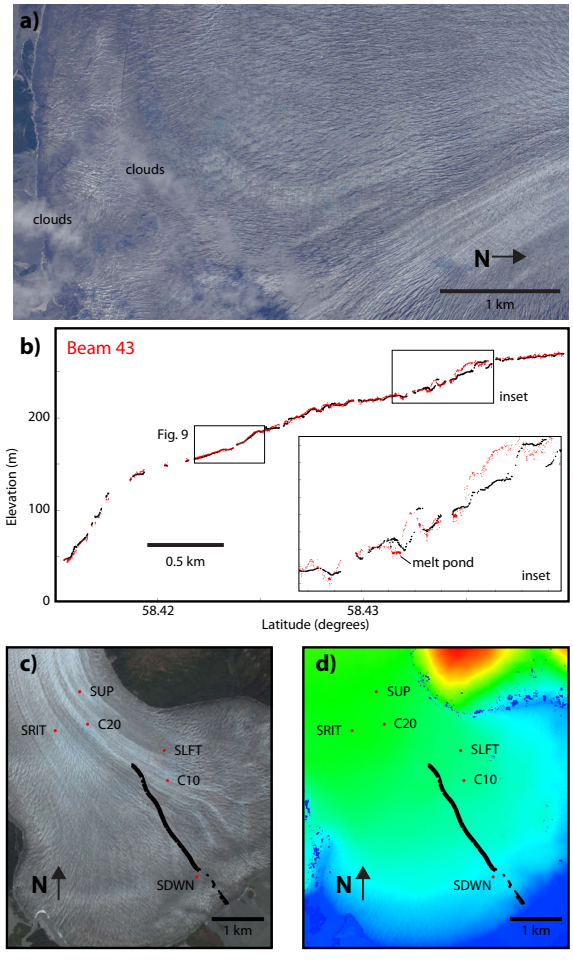

Figure 8. MABEL data over crevasse fields on the Lower Taku Glacier. **(a)** Stitched MABEL camera images. **(b)** MABEL signal photons (red), migrated based on GPS data and corrected for an 8 m range bias, and elevations extracted from the WorldView-2 DEM (black). **(c)** WorldView-2 image (Copyright DigitalGlobe, Inc.) with MABEL flight line and GPS sites (red). **(d)** WorldView-2 DEM (Moratto et al., 2010) with MABEL flight line and GPS sites (red).

The Cryosphere Discuss., doi:10.5194/tc-2015-225, 2016
Manuscript under review for journal The Cryosphere
Published: 19 January 2016

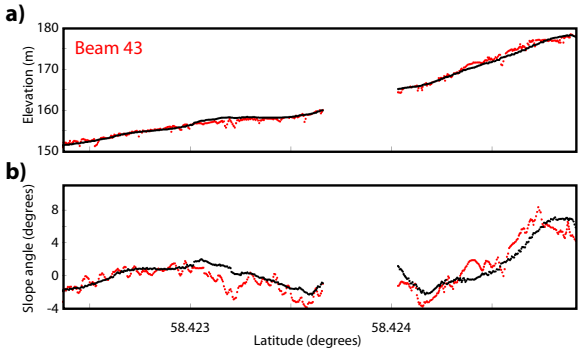

Figure 9. MABEL and DEM surfaces and slopes for a small stretch (see box in Fig. 8a) on the Lower Taku Glacier. **(a)** MABEL (red) and extracted DEM (black) elevations in m, for beam 43, migrated based on GPS data and corrected for an 8 m range bias. **(b)** MABEL (red) and DEM (black) across-track slope angle in degrees, using beams 43 and 50.